ACS APPLIED MATERIALS & INTERFACES

Article

Studies on bacterial proteins corona interaction with saponin imprinted ZnO nano-honeycombs and their toxic responses

Deepali Sharma, Md. Ashaduzzaman, Mohsen Golabi,
Amritanshu Shriwastav, Krishna Bisetty, and Ashutosh Tiwari

ACS Appl. Mater. Interfaces, **Just Accepted Manuscript** • DOI: 10.1021/acsami.5b06617 • Publication Date (Web): 06 Oct 2015

Just Accepted

ACS Publications

ACS Applied Materials & Interfaces is published by the American Chemical Society.
1155 Sixteenth Street N.W., Washington, DC 20036

Studies on bacterial proteins corona interaction with saponin imprinted ZnO nano-honeycombs and their toxic responses

Deepali Sharma[1,†], Md. Ashaduzzaman[2,†], Mohsen Golabi,[2] Amritanshu Shriwastav[3], Krishna Bisetty[1], Ashutosh Tiwari[2,4*]

[1]Department of Chemistry, Durban University of Technology, P.O. Box 1334, Durban 4000, South Africa

[2]Biosensors and Bioelectronics Centre, IFM, Linköping University, Linköping 58183, Sweden

[3]Department of Civil Engineering, Indian Institute of Technology Kanpur, Kanpur 208016, Uttar Pradesh, India

[4]Tekidag AB, UCS, Teknikringen 4A, Mjärdevi Science Park, Linköping 58330, Sweden

[†] The authors contributed equally.
*Corresponding author.
E-mail: ashutosh.tiwari@liu.se, Tel: (+46) 13-28-2395 and Fax: (+46) 13-13-7568.

ABSTRACT

Molecular imprinting generates robust, efficient and highly mesoporous surfaces for bio-interactions. Mechanistic interfacial interaction between the surface of core substrate and protein corona is crucial to understanding the substantial microbial toxic responses at a nanoscale. In this study, we have focused on the mechanistic interactions between synthesised saponin imprinted zinc oxide nano-honeycombs (SIZnO NHs), average size 80-125 nm, surface area 20.27 m^2/g, average pore density 0.23 pore/nm and number average pore size 3.74 nm and proteins corona of bacteria. The produced SIZnO NHs as potential anti-fungal and anti-bacterial agents have been studied on *Sclerotium rolfsii (S. rolfsii)*, *Pythium debarynum (P. debarynum) and Escherichia coli (E. coli)*, *Staphylococcus aureus (S. aureus)*, respectively. SIZnO NHs exhibited the highest antibacterial (~50%) and antifungal (~40%) activity against gram-negative bacteria (*E. coli) and fungus (P. debarynum)* respectively at concentration of 0.1 mol. Scanning electron spectroscopy (SEM) observation showed that the ZnO NHs ruptured

the cell wall of bacteria and internalised into the cell. The molecular docking studies have been carried out using *lipopolysaccharide* and *lipocalin Blc* as binding proteins. It was envisaged that the proteins present in the bacterial cell wall were found to interact and adsorb on the surface of SIZnO NHs thereby blocking the active sites of the proteins used for cell wall synthesis. The binding affinity and interaction energies for *lipopolysaccharide* were higher than those of the *lipocalin Blc*. In addition, a kinetic mathematical model (KMM) was developed in MATLAB to predict the internalisation in the bacterial cellular uptake of the ZnO NHs for better understanding of their controlled toxicity. The results obtained from KMM exhibited a good agreement with the experimental data. Exploration of mechanistic interactions, as well as the formation of bioconjugate of proteins and ZnO NHs would play a key role to interpret more complex biological systems in nature.

KEYWORDS: ZnO nano-honeycombs, protein corona, interaction energies, molecular docking, microbial toxicity.

BRIEFS: Nanobio-interface of saponin imprinted zinc oxide nano-honeycombs and microbial proteins adversely suffers from electrostatic forces, rate of adsorption, production of reactive oxygen species, rate of penetration and exposure time which are capable of responding to control the toxicity of medium.

INTRODUCTION

Nanoscale approaches are immensely involved with the advanced materials engineering for their high-performance and efficient applications.[1,2] The toxic effect of nanoscale materials on living organisms and biological systems are an extremely hot area of research.[3-5] Study of nanotoxicity in microbial systems holds importance because of their diversity and antimicrobial activity to explore applications in medical science which demands the need of understanding their interactions with membrane proteins, DNA and various biomolecules inside the cells. Typically, toxic effects based on advanced architectural and functionalized nanomaterials for example ZnO, silver, and gold are widely focused due to their less-toxic and cellular

compatibility with excellently tuned luminescence property. They can be used in biomedical and pharmaceutical applications including drug delivery and bio-imaging.[6-8] However, the knowledge about the mechanistic interactions and the toxic effects of nanoscale materials on biological systems is a challenge.

Recently, cellular toxicity of ZnO nanoparticles (NPs) in terms of particle size, concentration, dose-dependent oxidative stress, intracellular dissolution, bioavailability of Zn^{2+} has been studied intensively.[9-15] Toxic effects also include the morphological structure of NPs which is mainly dependent on the synthesis techniques. The synthesis of inorganic NPs using various biological materials like natural polymers is environment-friendly and termed as green method because they are biodegradable and bio-absorbable with degradation products that are non-toxic.[16-22] Synthesis of molecularly imprinted nanostructures has attracted much attention due to their multifarious potential applications including sensors, separations, catalysis and environmental management. Molecular imprinting is a technique used to create guest–complementary binding sites, mostly in a cross-linked polymer matrix.[23] Cross-linking of self-assembled functional moulding agents to construct the structural size and shape of template molecule via physical interaction provides molecularly imprinted desired structural dies. In this study we have fabricated ZnO nano-agglomerate dies via self-assembly of $Zn(OH)_2$ on saponin micelle used as a template molecule where metallic bonds within ZnO NPs formed upon irradiation of micro-wave resulted in an NHs structure having three-dimensional cavities. Secondly, we have reported the bacterial proteins corona interactions with SIZnO NHs towards the elucidation of their toxic responses by experimental and computational (molecular docking, mathematical model) studies.

In order to explore the mechanism of interaction between proteins and SIZnO NHs, it is highly important to understand the behaviour of NHs at the interface. The nanobio-interface comprises of the surface of NHs, its physicochemical properties, the solid-liquid interface and changes that occur when NHs interacts with any biological membrane. The nanobio-interface is constantly subjected to the influence of dynamic environment that actively contributes to its formation. When the biological components bind to the surface of the NHs, conformational changes occur due to the generation of reactive oxygen species (ROS) (Fig. S4).[24] The underlying interaction of NHs with the biological membranes is key to the understanding of their biological impact and to know their toxic effects.[25]

Nowadays, computational studies have become more popular to better understanding and to explain elaborately the mechanism involved in real biological systems. Molecular docking is one of the techniques widely used to comprehend the interaction of NPs with biological entities.[26-28] Park *et al.*[26] showed that fullerenes as well as single- walled carbon nanotubes (SWCNT) with an average diameter between 0.7 and 0.9 nm can "sit" on the top of a potassium channel (KcsA) and block the entrance for K^+ ions. The binding of the channel is not only affected by the size but also by the shape of the NPs. Atomistic molecular dynamics (MD) simulation studies by Kraszewski *et al.*[27] suggested that the binding of C60 fullerenes to different K^+ channels (KcsA, Kv1.2 and MthK) mainly depends on their size and hydrophobicity. Furthermore, human serum albumin and gold nanoparticle docking was carried out by Ramezani and Rafii-Tabar[28] and the complex with the best binding energy score (14.82 kcal mol^{-1}) was used for simulation and concluded that the free binding energy is equal to the intermolecular energy. Here, *lipopolysaccharide* and *lipocalin Blc* were selected for docking the proteins present in gram- negative bacteria with ZnO NHs. Finally, a kinetic mathematical

model was developed to predict the internalisation in bacterial cellular uptake of the NHs for better understanding of their controlled toxicity.

EXPERIMENTAL

Materials and methods

$ZnSO_4.7H_2O$, NaOH and saponin procured from SdFine and were used as received. Fungi (*P. debarynum*, *S. rolfsii)* and bacteria (*E. coli* and *S. aureus)* were collected from the Department of Basic Sciences, Dr. Y. S. Parmar University of Horticulture and Forestry, Nauni (Solan) India. Ultra pure water from ELIX 3Millipore was used as a solvent. A microwave (LG Model MB394AA, Power of 1200W, frequency 2.45 GHz), ultasonicator (Ultrasonic Bath Sonicator 3.5 L(H), LOBA Life), magnetic stirrer (Flexstir- FSH3 JSGW) and water were used for the synthesis of ZnO NHs. All the glassware and materials used for antimicrobial activity were sterilised in an autoclave for 20 min. before use to prevent contamination. Characterization and studies on surface morphology were carried out with X-ray diffractometer (PANalytical), transmission electron microscope (Hitachi S 7500), and Braunauer-Emmett-Teller (BET) analyser (Model Smart Sorb 92/93).

Synthesis of SIZnO NHs

$ZnSO_4.7H_2O$ and NaOH aqueous solutions were added in a molar ratio of 1:4 in a reaction flask. To this mixture, 0.5% (w/v) aqueous solution of saponin was added, and the resulting mixture was stirred vigorously for 15 min. The reaction mixture was exposed to microwave irradiation (microwave oven operating at 100% power of 1200 W and frequency 2.45 GHz) for 2 min. The white product obtained was thoroughly washed with copious distilled water and

ethanol. After ultrasonication, the product was washed again with distilled water and then dried at 60 ^{o}C till a constant weight was obtained.

Anti-microbial activity

The antifungal and antibacterial activities of the synthesised SIZnO NHs were done as reported in our previous paper.[29] The bits of grown fungi were put on the agar medium in respective petri-dishes without SIZnO NHs (control) and the other containing colloidal solution of the SIZnO NHs in different concentrations. The process was carried out in the horizontal laminar air flow. The samples were kept for 3-4 days at a temperature of 28 ^{o}C ± 2 ^{o}C to find out the antifungal activity. For each sample, 3 sets of replicates were carried out. For antibacterial activity, strains of gram-negative (*E. coli)* and gram positive (*S. aureus)* bacteria were grown in the nutrient medium (agar medium). The NHs free medium was used for a control experiment. The number of colonies formed was counted manually after 24 hrs of incubation at 37 ^{o}C.

Docking studies

The docking studies were carried out using DISCOVERY STUDIO (DS) 4.0.[30] The structures of *lipopolysaccharide* and *lipocalin Blc* binding proteins were obtained from the Protein Data Bank files. The proteins contained two subunits and for the purpose of this study, only one subunit was selected. First water molecules were removed, and hydrogen atoms were added. The protein molecules were cleaned to add missing hydrogen atoms or to remove alternate conformations. The binding sites in the molecules were determined using the receptor cavities option in DS 4.0. ZnO nanostructure was initially prepared in MATERIALS STUDIO 7 and opened as a ligand molecule in DS 4.0. It was prepared using the prepare ligand option. Finally, both protein molecules were docked separately onto the ligand using the CDOCKER molecular docking method in DS 4.0.

Parameters used in mathematical model for internalisation of NHs

To predict the dynamics of NHs internalised in *E. coli* and *S. aureus*, a mathematical model was developed following GEAR method using MATLAB. GEAR method has higher calculation efficiency and precision compared to other numerical methods therefore; the numerical solutions of dynamic differential equations have been obtained from GEAR method (see supporting information). The model parameters obtained from literature[31] are: forward rate constant ($k_f = 7.2 \times 10^{-7}$ mol^{-1} min^{-1}), reverse rate constant ($k_r = 0.34$ min^{-1}), endocytosis rate constant ($k_e = 1.14 \times 10^{-6}$ min^{-1} for *E.coli* and 7.70×10^{-6} min^{-1} for S. aureus), rate with which either NHs accumulate inside cell/recycled back to the membrane ($k_{rec} = 0.005$ min^{-1}), active reaction sites on the cell surface ($R_s = 1 \times 10^5$, assumed within literature reported range), rate of intracellular toxicity (($k_t = 4.6x10^{11}$ cell mol^{-1} min^{-1} (toxicity of intracellular nano to bacteria cells)) (optimized using least square method), and Avagadro's number ($N = 6.022 \times 10^{23}$).

RESULTS AND DISCUSSION

Synthesis and characterization of SIZnO NHs

SIZnO NHs was synthesised by microwave irradiation of the reaction mixture, $ZnSO_4.7H_2O$ and NaOH with molar ratio of 1:4 in the presence of 0.5% w/v aqueous saponin solution as shown in the schematic Fig. 1. The suspended $Zn(OH)_2$ was self-assembled onto the micelle of saponin which was exposed to microwave irradiation. The micelle with initially grown ZnO NPs was agglomerated due to their inherent liphophilic affinity. There were two possible routes leading to the formation of honeycombs morphology. Nucleation and agglomeration of NPs may occur separately or simultaneously due to high energy microwave irradiation where possibly metallic bonds formed quickly within ZnO NPs. In addition, microwave also facilitated

to detach saponin mostly from agglomerated NHs due to vibrational energy. The remaining saponin was removed by washing with good solvents (ethanol and water). Prior to biological testing, the SIZnO NHs were characterised spectroscopically. Powder X-ray diffraction (XRD) spectra confirmed that the ZnO nanocrystal units of SIZnO NHs had a hexagonal wurtzite type crystal structure (Fig. S1). The mesoporous rough surface of the SIZnO NHs was controlled by lowering of surface energy due to adsorption of single or multi sugar chains bearing glycosides. The adsorption, desorption curves and surface area of SIZnO NHs were obtained directly from the BET analyser using nitrogen adsorption (Fig. S2). The surface area of the SIZnO NHs was calculated to be 20.27 m^2/g.

For an advanced engineering of ZnO NHs with favourable bioavailability and biodistribution, it is essential to have an in-depth knowledge of the mechanism(s) of association and interaction of proteins with the particle surface and the consequent effect on the structure of the protein. Towards achieving this goal, an antimicrobial activity of SIZnO NHs was tested against two different fungi and bacteria. SEM observations were also carried out to visualise interaction phenomena between the bacterial cell wall and ZnO NHs. The explanation for the mechanistic interaction between SIZnO NHs and bacterial cellular proteins was further supported by protein docking studies and dynamic mathematical model developed in MATLAB.

Anti-microbial activity of SIZnO NHs

The anti-microbial activity of SIZnO NHs was tested with two different fungi and bacteria. Figs. 2(a-b) exhibit the antifungal activity of commercial SIZnO NHs against *S. rolfsii* and *P. debarynum*. The both fungi were exposed to SIZnO NHs at concentrations ranging from 2×10^{-2} to 10×10^{-2} mol L^{-1}. It was evident that there was no activity against the fungi at the lowest

concentration of honeycombs but about 20% activity was observed in case of *P. debarynum* at 4×10^{-2} mol L^{-1}. The average activity of the honeycombs against *P. debarynum* is higher than that of *S. rolfsii.* At the maximum concentration (10×10^{-2} mol L^{-1}) of NHs experienced in the test, the antifungal activity against *S. rolfsii* and *P. debarynum* was found to be 23.08% and 52%, respectively. Here, SIZnO NHs act on pathogenic microbes by inhibiting an enzyme-catalysed reaction present in the fungal cells. They also inhibit cell wall synthesis thereby causing fungal cell lysis (bursting) and death due to the structural change of corona proteins.[32] The mechanism involved with the cytotoxicity of nanostructures has been attributed to interaction with the plasma membrane of the fungal cells to affect the membrane permeability which has fatal results for the cell. They might also disrupt protein synthesis required for the survival of the fungus or inhibit nucleic acid function thereby preventing cell divisions or the synthesis of essential enzymes.[33]

Besides, Figs. 2(c-d) exhibit antibacterial activity against *E. coli* and *S. aureus* over the same concentration range of NHs used for fungi. The NHs was active against both of the bacteria for all concentrations, but average activity against *E. coli* (40%) was found to be superior to that of *S. aureus* (22.14%). The percentage reduction of bacteria (R%) has been calculated using the following equation:[34]

$$R\% = (B-A)\times100/B \quad \text{----------} \quad \text{(i)}$$

Where, B is the number of colonies forming units (cells) in control, and A is the number of cells in treated specimen after inoculation over 24 hrs contact period.

The better antibacterial activity of ZnO NHs against *E. coli* as compared against *S. aureus* has been explained in details in terms of bacterial cell wall constituents, types and construction. Peptidoglycans are the structural elements of almost all bacterial cell walls. They

constitute almost 95% of the cell wall in gram-positive bacteria and around 5% of the cell wall in gram-negative bacteria. The cell wall in gram-positive bacteria (*S. aureus*) is thick, consisting of several layers of peptidoglycan complex with molecules called teichoic acids whereas in gram-negative bacteria (*E. coli*), the cell wall is thin and is composed of a thin layer of peptidoglycan adjacent to the cytoplasmic membrane. When SIZnO nanostructures come into contact with the bacterial cell wall, they cause the disruption of the cell membrane by the production of ROS such as superoxide and hydroxyl radicals, generating a positive zeta potential, created by an electromagnetic interaction between the microbial surface and the NHs. Since, SIZnO NHs has positive zeta potential it easily penetrates into the thin cell wall of the gram-negative bacteria (*E. coli*) which has negative charges on its membrane. This rupture the membrane releasing toxic Zn^{2+} ions causing cell wall damages finally leading to the static growth/death of bacteria.[35] SIZnO nano-structures inactivate the proteins present in the cell membrane of the bacteria thereby retarding the adhesion of bacteria. In *S. aureus*, the cell wall is thick and, therefore the honeycombs are not able to easily penetrating the cell membrane. A repulsive force is generated as the NHs comes in contact with the cell membrane resulting in the generation of reactive oxygen species (ROS).[36,37]

In Fig. 2d, it has been observed that at higher concentration of SIZnO NHs, the value for the % reduction of bacteria was constant. It may be due to the fact that at the interface of the microbial membrane, the SIZnO nanostructures are aggregated thereby, resulting in an almost constant antibacterial activity at the higher concentration of ZnO NHs. An interaction of SIZnO NHs with bilayer at nanobio-interface and cleavage of a cell wall structure of gram-positive bacteria is schematically presented in supporting information (Fig. S3).

In Fig. 3 morphological characterisation of ZnO NHs and interaction phenomena with different bacteria have been elaborately discussed. TEM image revealed almost homogeneously distributed mesoporous honeycombs like ZnO nanostructure with a diameter of around 80-125 nm, average pore density 0.23 pore/nm^2, number average pore (diameter) size 3.74 nm ((Fig. 3(a-a′)). In order to clarify the interaction between bacteria and ZnO NHs and to visualise its impact on the cell wall, SEM observations of bacteria with distinguished magnifications were captured without and with ZnO NHs. It is evident from the Fig. 3 b′ that only 2 hrs after addition of ZnO NHs (0.1 mol L^{-1}), a corona of hydrated ZnO NHs onto the cell wall of *E. coli* was developed and firmly attached to the surface. Therefore, the smooth cell wall of *E. coli* (Fig. 3b) was ruptured which is indicated by the arrow in Fig. 3b′. The inset magnified image also clearly showed the insertion of ZnO NHs inside of the cell wall. Similarly, *S. aureus* after addition of similar concentration of NHs was deformed from floppy-dumble shape to a squeezed-flattened sheet with adjoining one another due to immobilisation onto the substrate as shown in Fig. 3 (c -c′).

Molecular docking studies of ZnO NHs-protein corona interactions

The design of molecular docking studies was constructed for the exploration of mechanistic interaction between ZnO NHs and bacterial cell membranes containing binding proteins (lipopolysaccharide, lipocalin Blc, protein A and C-domain of protein A). Fig. 4 illustrates the images for interaction between the crystal structures of the lipopolysaccharide binding protein (LBP, PDB ID 4M4D), lipocalin Blc (PDB ID 1QWD), protein A (PDB ID 2JWD) and C-domain of protein A (PDB ID 4NPE) taken from RCSB protein data bank[37, 38] with ZnO NHs. These crystal structures were considered because of their existence in the cell wall of gram negative and gram positive bacteria, respectively.

Gram negative bacteria contain lipopolysaccharides (LPS) in their outer cell wall. LBP are considered to play a major role in regulating LPS dependent monocyte responses whereas lipocalin Blc (outer membrane protein) present in *E. coli* is capable of phospholipid binding and lipid transport[39].

Staphylococcal protein A (SpA) is highly abundant 42 kDA surface protein found in the cell wall of bacterium *Staphylococcus aureus* and encoded by the *spa* gene. It has two distinct halves, the C-terminal which binds Spa to the extracellular surface of the peptidoglycan cell wall and N-terminal which is a series of five stable protein binding domains (E-D-A-B-C). As a pathogen, *S. aureus* utilizes protein A for its survival and virulence.[40]

Nanostructures interact with biomolecules like proteins, lipids, enzymes due to their high surface to volume ratio. Of special interest is the adsorption of the proteins on the surface of the nanomaterials thereby forming nanoparticle-protein corona (NP-PC). NP-PC is reported to influence the biological activity of the nanoparticles.[41] Here ZnO nanocluster was docked with the protein molecules to speculate the nanobio-interface interactions and the active sites in these proteins were found in the receptor cavities. In the case of *lipopolysaccharide* binding protein (LBP) and *lipocalin Blc* there were 10 poses for each (Tables S1 and S2) whereas there were 3 poses for staphylococcal protein A and 2 poses for C-domain of protein A (Tables S3 and S4). The Cdocker and interaction energies for all poses in the case of the all the proteins are summarized. The higher values of the Cdocker and the interaction energies suggested a more favourable binding of the Zn and O atoms. In LBP, Zn atoms were approached to bind with oxygen of proline (PRO265), threonine (THR263), leucine (LEU101), valine (VAL140) and proline (PRO451). Fig. 4 (a, b) suggests that the oxygen atom of the ZnO nanocluster does not

interact with amino acids. Fig. 4 (c, d) depicts the interaction of Zn and O atoms of the ZnO NHs with the amino acids of *lipocalin Blc* protein. Zn atoms of NHs attached with oxygen atoms of glutamic acid (GLU90), phenylalanine (PHE109), aspartic acid (ASP134, 136) and valine (VAL30, 31), respectively. It was noted that the oxygen of the honeycombs also interacted with glutamic acid (GLU54) and threonine (THR146). The higher value of receptor-ligand energies of *lipocalin Blc* protein indicated stronger binding affinity than that of LBP.

Fig. 4 (e, f) depicts the binding site of nanocluster with the protein molecule (Protein A). On docking, the Zn atom of the nanocluster bound with oxygen atom of aspartic acid (ASP1, SP3) and valine (VAL2); asparagine (ASN7); asparagine and glutamic acid (GLU26); glutamic acid and asparagine (GLU16, ASN12). The oxygen atom bound to hydrogen of valine and nitrogen of asparagine (VAL2, ASP1); hydrogen of phenylalanine (PHE14) and glutamine (GLN27, GLN56). The binding of Zn and O atoms of the nanocluster with the C-domain of Staphylococcal protein A is depicted in Fig. 4 (g, h). Among different domains of Protein A, ZnO nanocluster bound to C-domain only. Here, Zn atom of the nanocluster bound to the oxygen atom of aspartic acid (ASP36, ASP37); lysine and asparagines (LYS4, ASN3); tyrosine and glutamic acid (TYR14, GLU15); threonine and glutamic acid (THR23, GLU24) whereas O atom of the nanocluster bound to hydrogen of histidine and tyrosine (HIS18, TYR14); phenylalanine and asparagines (PHE5, ASN6); glutamine (GLN32). The values of Cdocker and interaction energy for C-domain were found to be less as compared to Protein A.

In the case of gram positive bacteria, not all the atoms of the ZnO nanocluter were docked with the atoms of the amino acids which can be visualized in Figs. 3f and 3h. The reason might be that the values of Cdocker and Cdocker interaction energies are not high as

compared to that of proteins present in the cell wall of gram negative bacteria. As a result, the nanoparticles are not able to interact with the Protein A present in the extracellular surface of the cell wall. The direct comparison of the docking studies carried out in the case of gram negative and gram positive bacteria have been tabulated in Table 1. As a higher (positive) value of–Cdocker energy and –Cdocker interaction energy indicates a favourable binding thus, the higher values in the case of proteins of gram negative bacteria as compared to the gram positive bacteria as seen in the Table 1 leads to the conclusion that atoms of the ZnO NHs bind more effectively to the membrane proteins of the gram negative bacteria.

Table 1. Comparison of docking studies of gram negative and gram positive bacteria

Component	**Gram negative bacteria**		**Gram positive bacteria**	
Proteins in the cell wall	Lipopolysaccharide binding protein (LBP)	Lipocalin Blc	Protein A	C-domain of Protein A
Cdocker energy (Kcal/mol)	-61.0053	-86.2237	-31.0746	-24.9807
Cdocker interaction energy (Kcal/mol)	-54.3061	-80.9758	-31.9003	-25.1463
No. of poses	10	10	3	2
Binding of Zn atoms of the nanocluster with amino acids of the protein	PRO265, THR263, LEU101, VAL140, PRO451	GLU90, PHE109, ASP134, ASP136, VAL30, VAL31	ASP1, ASP3, VAL2, ASN7, GLU26, GLU16, ASN12	ASP36, ASP37, LYS4, ASN3, TYR14, GLU15, THR23, GLU24
Binding of O atoms of the nanocluster with amino	-	GLU54,	VAL2, ASP1,	HIS18, TYR14,

acids of the protein	THR146	PHE14, GLN27, GLN56	PHE5, ASN6, GLN32

Dynamics of SIZnO NHs internalised in bacteria

The understanding of fundamental physicochemical properties of the nanomaterials towards different cellular responses presents important contributions to the progressive exploration of cytotoxicity paradigm, which requires constant refinement and updating with the discovery of novel nanobio-interactions.[42] The effects of Trojan horsetype nanoparticle transport and oxidative stress-induced cellular damage are well-established within these paradigms.[13,43,44] The cellular internalisation of the nanoparticles followed by intracellular dissolution results in further cytotoxicity. However, such model is non-universal and is dependent on the relative rates of dissolution of the nanoparticles with respect to that of cellular uptake. In this model, the following equations were used to predict the internalisation of NHs, which are modified to include the toxic effects of surface and internalised nanostructures. Bulk phase ZnO NHs $(dL/dt) = (-k_a \times L + k_r \times c_s) \times (n/N)$, concentration of NHs on the cell surface $(dc_s/dt) = k_a \times L - (k_r + k_e) \times (c_s + k_{rec} \times c_i) - (k_d \times c_s)$, concentration of NHs inside the membrane: intracellular concentration $(dc_i/dt) = k_e \times c_s - (k_{rec} \times c_i) - (k_d \times c_i)$, $k_a = k_f \times R_s\ (n/N)$, $k_d = k_t \times (c_i/n)$ and $dn/dt = -k_d \times n$. Where, L represents the bulk concentration of ZnO NHs, c_s is the concentration of NHs on the cell surface, c_i is the intracellular concentration of nanocluster and cell density (number of cells/L) is given by dn/dt. The value of k_t was optimized using error minimization by least square method.[45] Using above equations, reduction cell density of bacterial (*E. coli* and *S. aureus*) due to toxicity of ZnO NHs were plotted against time and correlated with experimental results.

The number of cells in control were $2.5x10^5$ (*E. coli*) and $2.8x10^5$ (*S. aureus*) cells/L as shown in Figs. 5(a-b). As the time progressed there was a reduction of cell density with the increase of the concentration of ZnO NHs. The experimental values of cell density were accounted from the percentage reduction of bacterial after 24 hrs in each case. For example, in case of 0.04 M ZnO NHs, 20 and 10.7% of initial *E. coli* and *S. aureus* concentrations were reduced and the resulted concentrations were found to be 2.0×10^5 and 2.5×10^5 cells/L. It is evident that the experimental and simulated results are consistent in the case of *E. coli* whereas slight deviations were observed in case of *S. aureus* which is attributed to the fact that since, *S. aureus* is a gram-positive bacteria the reduction in bacterial cells is becoming constant and does not change significantly at higher concentration of ZnO NHs.

The concentrations of ZnO NHs on the surface (c_s) and inside (c_i) the bacterial cell were calculated using mathematical model to evaluate theoretically the amount of nanostructures which cross the surface and reach within the cell ((Fig. S4 (X-Y)). The highest concentration of NHs was observed at 600 minutes. Here, Fig. 6 (a- b) illustrates the highest ZnO concentrations onto the outer surface and inside of bacterial cell corresponding to the applied concentration of ZnO NHs. It is envisaged from Fig. 6 (a) that *S. aureus* showed higher adsorption of ZnO compared to *E. coli,* and the values were increased with the increase of concentrations. Besides, due to the difference in cell wall thickness and compositional discrepancies, the penetration of NHs through *E. coli* cell interface was found higher than that of *S. aureus* as shown in Fig. 6 (b). The percentage molar concentration of ZnO into the cell was calculated to be about 0.02 with respect to the corresponding accumulated concentration onto the surface of the cell wall in all cases. Although with increasing ZnO NHs concentrations, adsorption and penetration rates

for *E. coli* and *S. aureus* were found an opposite relationship which can be realised by measuring the relative slopes from the trend lines.

CONCLUSION

A unique green synthesis route for saponin imprinted ZnO NHs was established. These NHs were highly active against both *P. debarynum* and *E. coli* at concentration 10×10^{-2} mol L^{-1}. The interaction mechanisms involved with the system were electrostatic, adsorption and diffusional penetration promoted by functional groups present in proteinous microorganisms, their cell wall thickness and concentration of NHs. The NHs was found to block the active sites of the proteins present in the cell wall thereby inhibiting the enzymatic synthesis of a bacterial cell which was supported by molecular docking studies. The binding affinity and interaction energies were greater for *lipocalin Blc*, thus suggesting a stronger interaction of the ZnO NHs with the *E. coli*. Additionally, to understand the antimicrobial activity of nanostructures at a cellular level, a facile kinetic mathematical model has been proposed where endocytosis rate of NHs was predicted. It was also proved that an increasing the concentration of ZnO NHs resulted in a reduction of the number of bacterial cells. These combined phenomena would play a vital role to explore core-corona interfacial interaction mechanisms at a nanoscale in more complex biological systems.

ACKNOWLEDGEMENT

The authors wish to acknowledge the Swedish Institute (SI ref. 00037/2014) for an exchange program to carry out this research.

SUPPORTING INFORMATION includes an antimicrobial activity, XRD and BET, SEM analysis of saponin imprinted ZnO nano-honeycombs. The results of ZnO NHs interactions and cell wall cleavage, representation of an interaction of NHs with bilayer at nanobio-interface and cleavage of a cell wall structure of gram-positive bacteria. The concentrations of ZnO NHs on the surface and inside of the bacterial cell wall have been calculated using the mathematical model to evaluate theoretically the amount of NHs, which cross the surface and reach within the cell. Tables summarised the Cdocker and Interaction energies of different poses of *Lipopolycaccharide* as well as Cdocker and interaction energies of different poses of *Lipocalin Blc.* This information is available free of charge via Internet at http://pubs.acs.org.

REFERENCES

(1) Tiwari, A.; Mishra, A. K.; Kobayashi, H.; Turner, A. P. F. (Eds.) Intelligent Nanomaterials, First edition, *Wiley*-Scrivener, USA, 2012.

(2) Tiwari, A.; Tiwari, A. (Eds.) Bioengineered Nanomaterials, First edition, *CRC press,* USA, 2013.

(3) Adams, C. P.; Walker, K. A.; Obare, S. O.; Docherty, K. M. Size-Dependent Antimicrobial Effects of Novel Palladium Nanoparticles. *PLoS One* 2014, 9, e85981, 1-12.

(4) Ren, F.; Yang, B.; Jing Cai, Jiang, Y.; Xu, Jun.; Wang, S. Toxic Effect of Zinc Nanoscale Metal-Organic Frameworks on Rat Pheochromocytoma (PC12) Cells *in Vitro*. *J. Hazard. Mater.* 2014, 271, 283–291.

(5) Sharifi, S.; Behzadi, S.; Laurent, S.; Forrest, M. L.; Stroeve, P.; Mahmoudi, M. Toxicity of Nanomaterials. *Chem. Soc. Rev.* 2012, 41, 2323-2343.

(6) Rasmussen, J. W.; Martinez, E.; Louka, P.; Wingett, D. G. Zinc Oxide Nanoparticles for Selective Destruction of Tumor Cells and Potential for Drug Delivery Applications. *Expert Opin. Drug Delivery* 2010, 7, 1063-1077.

(7) Dutta, S.; Basak, S.; Samanta, P. K. Tunable Photoemission from Bio-compatible ZnO Quantum Dots and Effect of PVA. *Int. J. Nanosci. Nanotech.* 2012, 3, 27-32.

(8) Brown, P. K.; Qureshi, A. T.; Moll, A. N.; Hayes, D. J.; Monroe, W. T. Silver Nanoscale Antisense Drug Delivery System for Photoactivated Gene Silencing. *ACS Nano* 2013, 7, 2948-2959.

(9) Prach, M.; Stone, V.; Proudfoot, L. Zinc Oxide Nanoparticles and Monocytes: Impact of Size, Charge and Solubility on Activation Status. *Toxicol. Appl. Pharmacol.* 2013, 266, 19-26.

(10) Gilbert, B.; Fakra, S. C.; Xia, T.; Pokhrel, S.; Madler, L.; Nel, A. E. The Fate of ZnO Nanoparticles Administered to Human Bronchial Epithelial Cells. *ACS Nano* 2012, 6, 4921-4930.

(11) Shen, C.; James, S. A.; De Jonge, M. D.; Turney, T. W.; Wright, P. F. A.; Feltis, B. N. Relating Cytotoxicity, Zinc Ions, and Reactive Oxygen in ZnO Nanoparticle-Exposed Human Immune Cells. *Toxicol. Sci.* 2013, 136, 120-130.

(12) Deng, X.; Luan, Q.; Chen, W.; Wang, Y.; Wu, M.; Zhang H.; Jiao, Z. Nanosized Zinc Oxide Particles Induce Neural Stem Cell Apoptosis. *Nanotechnology* 2009, 20, 115101.

(13) Xia, T.; Kovochich, M.; Liong, M.; Madler, L.; Gilbert, B.; Shi, H.; Yeh, J. I.; Zink, J. I.; Nel, A. E. Comparison of the Mechanism of Toxicity of Zinc Oxide and Cerium Oxide Nanoparticles Based on Dissolution and Oxidative Stress Properties. *ACS Nano* 2008, 2, 2121-2134.

(14) De Berardis, B.; Civitelli, G.; Condello, M.; Lista, P.; Pozzi, R.; Arancia, G.; Meschini, S. Exposure to ZnO Nanoparticles Induces Oxidative Stress and Cytotoxicity in Human Colon Carcinoma Cells. *Toxicol. Appl. Pharmacol.* 2010, 246, 116-127.

(15) Sharma, V.; Anderson, D.; Dhawan, A. Zinc Oxide Nanoparticles Induce Oxidative Stress and Genotoxicity in Human Liver Cells (HepG2). *J. Biomed. Nanotechnol*. 2011, 7, 98-99.

(16) Jain, D.; Daima, H. K.; Kachhwaha, S.; Kothari, S. L. Synthesis of Plant-Mediated Silver Nanoparticles Using Papaya Fruit Extract and Evaluation of Their anti-Microbial Activities. *Dig J. Nanomater Biostruct.* 2009, 4, 557–563.

(17) Namvar, F.; Azizi, S.; Ahmad, M. B.; Shameli, K.; Mohamad, R.; Mahdavi, M. Tahir, P.M. Green Synthesis and Characterization of Gold Nanoparticles Using the Marine Macroalgae *Sargassum muticum. Res Chem Intermed*. 2015, 41, 5723-5730.

(18) Saifuddin, N.; Wong, C. W.; Yasumira. Rapid Biosynthesis of Silver Nanoparticles Using Culture Supernatant of Bacteria with Microwave Irradiation. *E- J. Chem*. 2009, 6, 61–70.

(19) Samat, N. A.; Nor, R. M. Sol–Gel Synthesis of Zinc Oxide Nanoparticles Using Citrus Aurantifolia Extracts**.** *Ceram. Int.* 2013, 39, 545–548.

(20) Singh, R. P.; Shukla, V. K.; Yadav, R. S.; Sharma, P. K.; Singh, P. K.; Pandey, A. C. Biological Approach of Zinc Oxide Nanoparticles Formation and its Characterization. *Adv. Mater. Lett.* 2011, 2, 313–317.

(21) Darroudi, M.; Ahmad, M.B.; Zamiri, R.; Zak, A.K.; Abdullah, A.H.; Ibrahim, N.A. Time-dependent Effect in Green Synthesis of Silver Nanoparticles. *Inter. J. Nanomed.* 2011, 6, 677–681.

(22) Darroudi, M.; Sarani, M.; Oskuee, R. K.; Zak, A.K.; Hosseini, H.A.; Gholami, L. Green Synthesis and Evaluation of Metabolic Activity of Starch Mediated Nanoceria, *Ceram. Int.* 2014, 40, 2041-2045.

(23) Yan, M.; Ramstrom, O. Molecularly Imprinted Materials Science and Technology, First edition, *Marcel Dekker*, New York, 2005.

(24) Nel, A.; Xia, T.; Madler, L.; Li, N. Toxic Potential of Materials at the Nanolevel. *Science* 2006, 311, 622-627.

(25) Alkilany, A. M.; Murphy, C. J. Toxicity and Cellular Uptake of Gold Nanoparticles: What We Have Learned so Far? *J. Nanopart. Res.* 2010, 12, 2313-2333.

(26) Park, K. H.; Chhowalla, M.; Iqbal, Z.; Sesti, F. Single-Walled Carbon Nanotubes are a New Class of Ion Channel Blockers. *J. Biol. Chem.* 2003, 278, 50212-50216.

(27) Kraszewski, S.; Tarek, M.; Tretow, W.; Ramseyer, C. Affinity of C60 Neat Fullerenes with Membrane Proteins: A Computational Study on Potassium Channels. *ACS Nano* 2010, 4, 4158-4164.

(28) Ramezani, F.; Rafii-Tabar, H. An In-Depth View of Human Serum Albumin Corona on Gold Nanoparticles *Mol. BioSyst.* 2015, 11, 454-462.

(29) Sharma, D.; Sharma, S.; Kaith, B. S.; Rajput, J.; Kaur, M. Synthesis of ZnO Nanoparticles Using Surfactant Free in-air and Microwave Method. *Appl. Surf. Sci.* 2011, 257, 9661-9672.

(30) Accelrys Software Inc. Discovery Studio Modeling Environment, Release 4.0, San Diego: *Accelrys Software Inc*., 2013.

(31) Jin, H.; Heller, D. A.; Sharma, R.; Strano, M. S. Size-dependent Cellular Uptake and Expulsion of Single-Walled Carbon Nanotubes: Single Particle Tracking and a Generic Uptake Model for Nanoparticles. *ACS Nano* 2009, 3, 149-158.

(32) Fleischer, C. C.; Payne, C. K. Nanoparticle-cell Interactions: Molecular Structure of the Protein Corona and Cellular Outcomes. *Acc. Chem. Res.* 2014, 47, 2651–2659.

(33) Patrik, G. L. *An Introduction to Medicinal Chemistry*, Second Edition. Oxford University Press 2001, 375-431.

(34) Anita, S.; Ramachandran, T.; Rajendran, R.; C.V.; Mahalakshmi, M. A study of the antimicrobial property of encapsulated copper oxide nanoparticles on cotton fabric. *Text. Res. J.* 2011, 81, 1081-1088.

(35) Huang, Z.; Zheng, X.; Yan, D.; Yin, G.; Liao, X.; Kang, Y.; Yao, Y.; Huang, D.; Hao, B. Toxicological Effect of ZnO Nanoparticles Based on Bacteria. *Langmuir* 2008, 24, 4140-4144.

(36) Sharma, D.; Kaith, B. S.; Rajput, J.; Sharma, S.; Kaur, M.; Rajendran, V.; Hillebrands, B.; Prabu, P.; Geckeler, K. E. (Eds.), *Biomedical Applications of Nanostructured Materials,* First edition, Macmillan Publishers India Ltd. India, 2010, 165-170.

(37) Eckert, J. K.; Kim, Y. J.; Kim, J. I.; Gurtler, K.; Oh, D. Y.; Sur, S.; Lundvall, L.; Hamann, L.; van der Ploeg, A.; Pickkers, P.; Giamarellos-Bourboulis, E.; Kubarenko A.V.; Weber, A. N.; Kabesch, M.; Kumpf, O.; An, H. J.; Lee, J. O.; Schumann, R. R. The Crystal Structure of Lipopolysaccharide Binding Protein Reveals the Location of a Frequent Mutation that Impairs Innate Immunity. *Immunity* 2013, 17, 647-660.

(38) Campanacci, V.; Nurizzo, D.; Spinelli, S.; Valencia, C.; Tegoni, M.; Cambillau, C. The Crystal Structure of the *Escherichia coli Lipocalin Blc* Suggests a Possible Role in Phospholipid Binding. *FEBS Lett.* 2004, 562, 183-188.

(39) Campanacci, V.; Bishop, R. E.; Blangy, S.; Tegoni, M. The Membrane Bound Bacterial Lipocalin Blc is a Functional Dimer with Binding Preference for Lysophospholipids. *FEBS Lett.* 2006, 280, 4877- 4883.

(40) Deis, L. N.; Pemble IV, C. W.; Qi, Y.; Hagarman, A.; Richardson, D. C.; Richardson, J. S.; Oas, T. G. Multiscale Conformational Heterogeneity in Staphylococcal Protein A: Possible Determinant of Functional Plasticity. *Structure* 2014, 22, 1467-1477.

(41) Saptarshi, S. R.; Duschl, A.; Lopata, A. L. Interaction of Nanoparticles with Proteins: Relation to Bio-reactivity of the Nanoparticle**.** *J. Nanobiotechnol.* 2013, 11, 1-12.

(42) Nel, A. E.; Mädler, L.; Velegol, D.; Xia, T. E.; Hoek, M. V.; Somasundaran , P.; Klaessig, F.; Castranova, V.; Thompson, M. Understanding Biophysicochemical Interactions at the Nano-bio Interface. *Nat. Mater.* 2009, 8, 543-557.

(43) Horie, M.; Nishio, K.; Fujita, K.; Kato, H.; Nakamura, A.; Kinugasa, S.; Endoh, S.; Miyauchi, A.; Yamamoto, K.; Murayama, H.; Niki, E.; Iwahashi, H.; Yoshida, Y.; Nakanishi, J. Ultrafine NiO Particles Induce Cytotoxicity in Vitro by Cellular Uptake and Subsequent Ni(II) Release. J. *Chem. Res. Toxicol*. 2009, *22*, 1415-1426.

(44) Gunawan, C.; Teoh, W. Y.; Marquis, C. P.; Amal, R. Cytotoxic Origin of Copper(II) Oxide Nanoparticles: Comparative Studies with Micron-sized Particles, Leachate, and Metal Salts. *ACS Nano* 2011, 5, 7214-7225.

(45) Alvarez-Guerra, M.; Ballabio, D.; Amigo, J. M.; Bro, R.; Viguri, J. R. Development of Models for Predicting Toxicity from Sediment Chemistry by Partial Least Squares-

Discriminant Analysis and Counter-propagation Artificial Neural Networks. *Environ. Pollut.* 2010, 158, 607–614.

Caption of the Figures

Figure 1. Schematic presentation of SIZnO NHs preparation process; step 1. Self-assembly of ZnO precursor and template, step 2. Nucleation and aggregation of molecularly imprinted saponin ZnO matrix, and step 3. Fabrication of SIZnO NHs via template removal.

Figure 2. Effect of saponin imprinted ZnO nano-honeycombs concentration on fungi (a) *S. rolfsii*, (b) *P. debarynum* and bacteria (c) *E. coli,* (d) *S. aureus*

Figure 3. TEM image of saponin imprinted ZnO NHs synthesised by microwave irradiation (a), distribution of pores on the surface (a′); SEM morphologies of *E. coli* and *S. aureus* before (b, c) and after addition of ZnO NHs (b′, c′) respectively.

Figure 4. Illustration of saponin imprinted ZnO NHs docking and interaction in binding sites with (a,b) *lipopolysaccharide*, (c,d) *lipocalin Blc* binding proteins, (e,f) Staphyloccocal protein A and (g, h) C-domain of protein A.

Figure 5. Changes of cell density in terms of experimental and simulated values with respect to time, (a) *E. coli* and (b) *S. aureus.*

Figure 6. Concentration of ZnO NHs (a) accumulated on the bacterial cell surface and (b) inside of the bacterial cell against the applied concentrations after 600 min.

Figure 1.

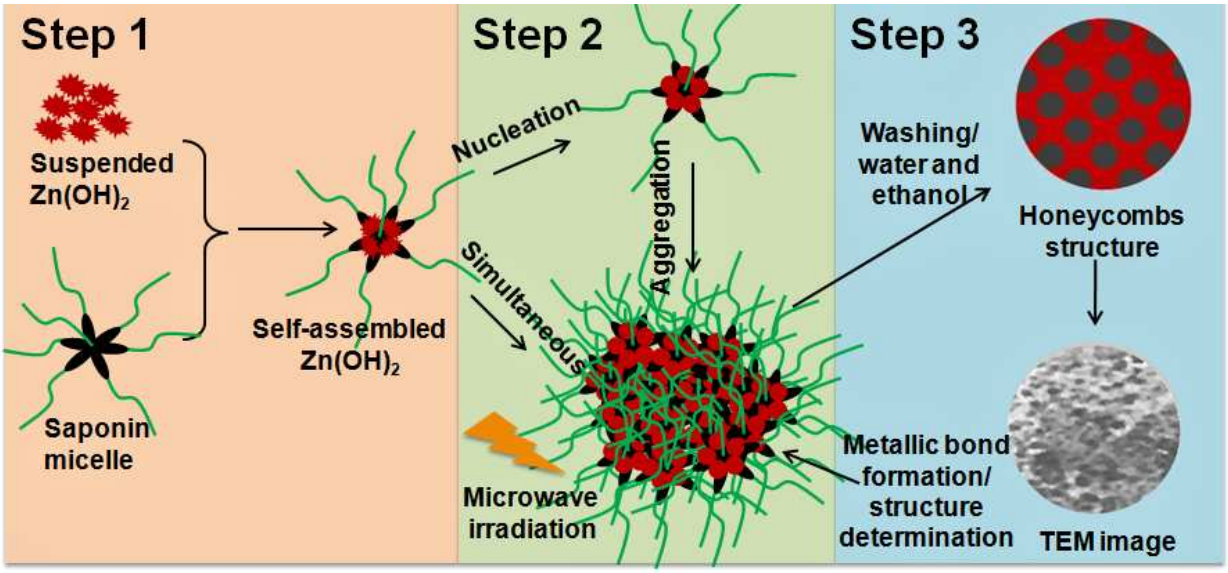
Step 1
Suspended $Zn(OH)_2$
Saponin micelle
Self-assembled $Zn(OH)_2$
Step 2
Nucleation
Aggregation
Simultaneous
Microwave irradiation
Step 3
Washing/ water and ethanol
Honeycombs structure
Metallic bond formation/ structure determination
TEM image

Figure 2.

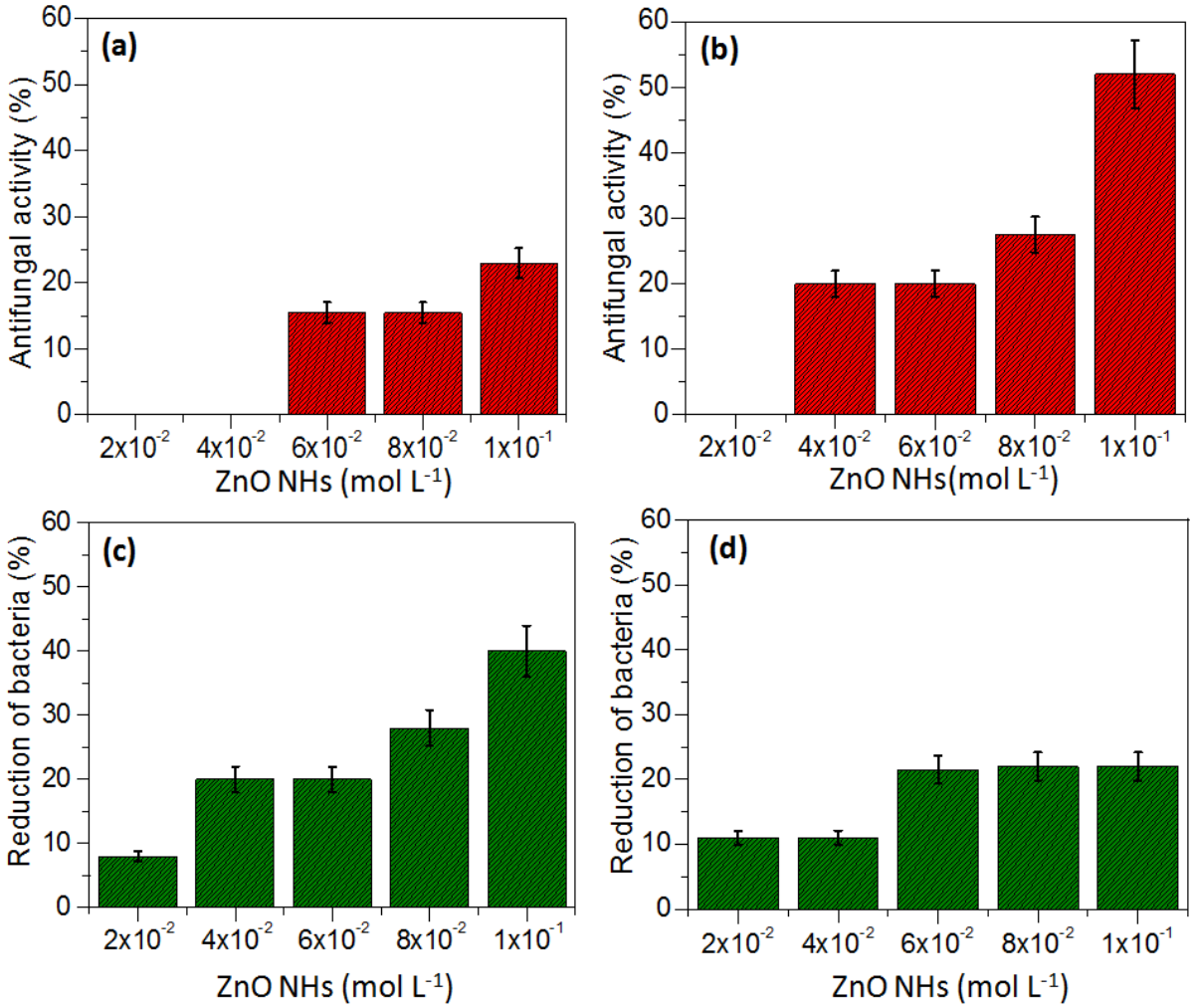
(a)
Antifungal activity (%)
ZnO NHs (mol L-1)
(b)
Antifungal activity (%)
ZnO NHs(mol L-1)
(c)
Reduction of bacteria (%)
ZnO NHs (mol L-1)
(d)
Reduction of bacteria (%)
ZnO NHs (mol L-1)
2x10-2
4x10-2
6x10-2
8x10-2
1x10-1
0
10
20
30
40
50
60

Figure 3.

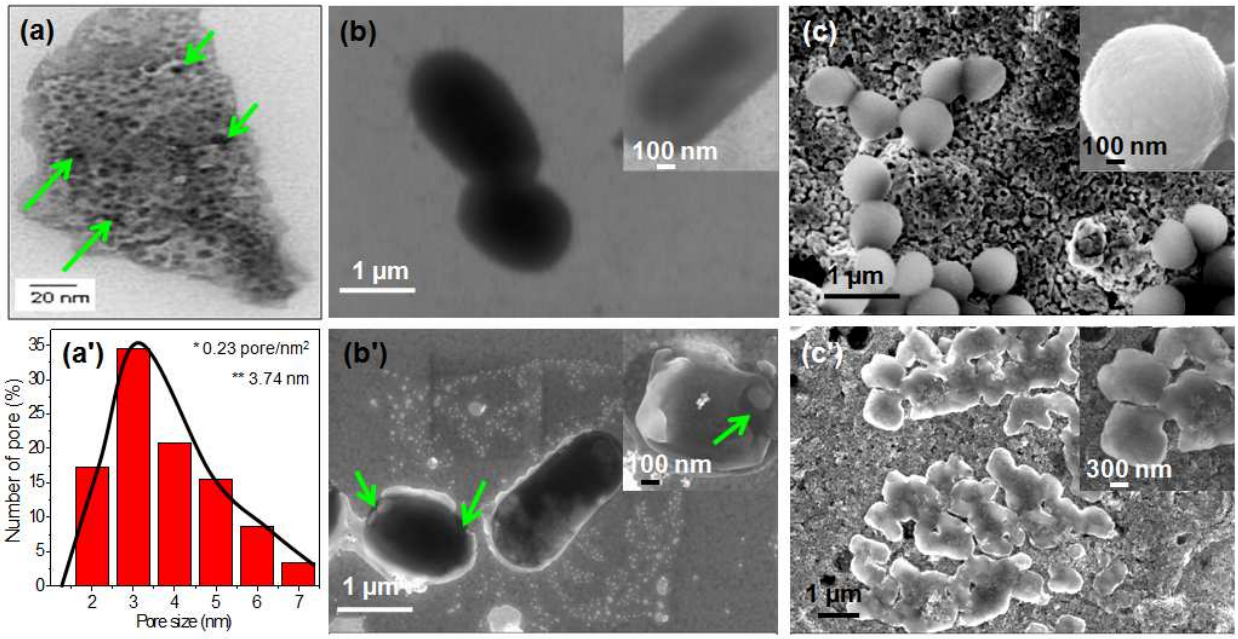

*Average pore density and **average pore size (diameter).

Figure 4.

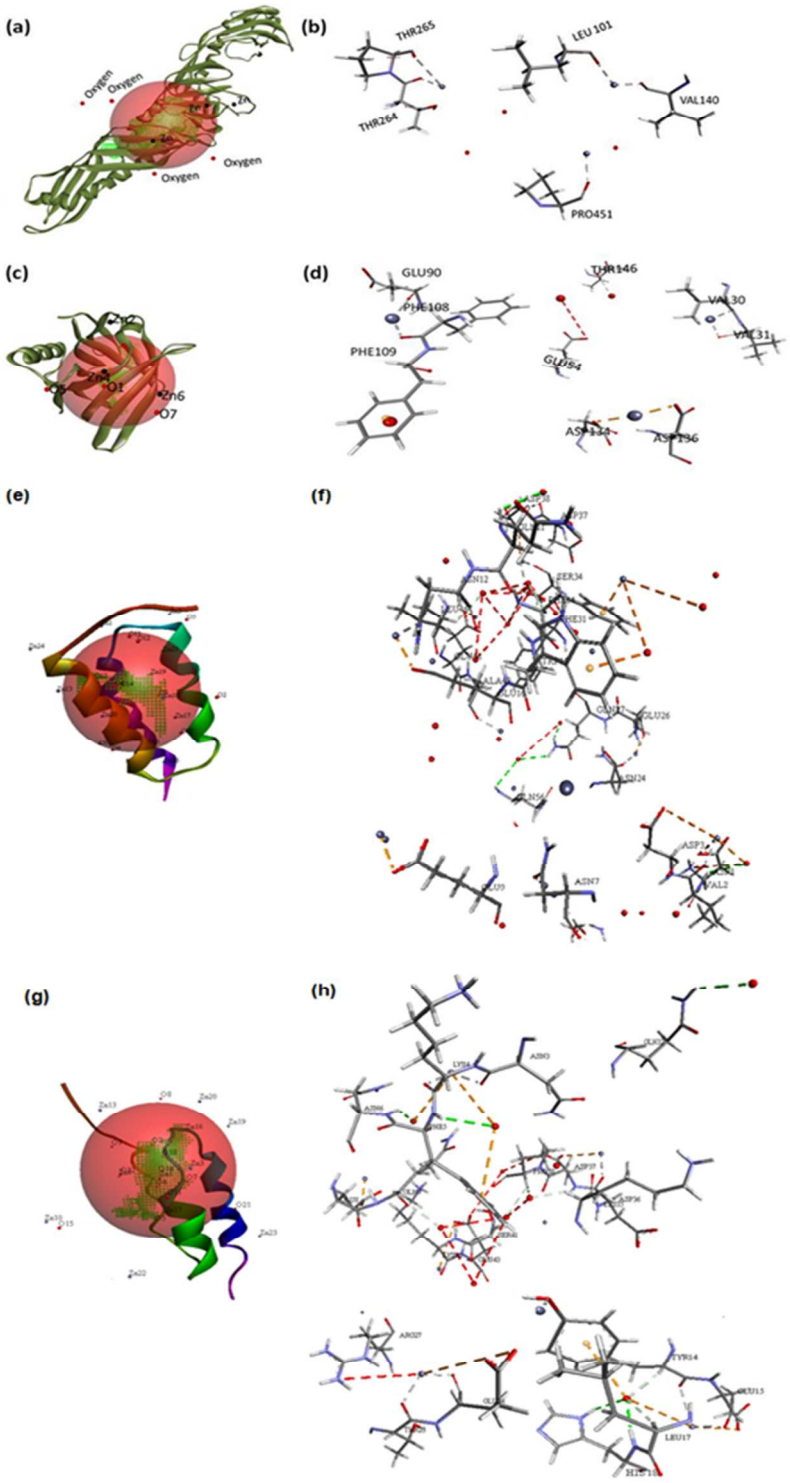
(a)
Oxygen
Oxygen
Oxygen
Oxygen
(b)
THR265
LEU 101
VAL140
THR264
PRO451
(c)
O1
Zn6
O7
(d)
GLU90
PHE108
PHE109
THR146
VAL30
VAL31
GLU54
ASP114
ASP196
(e)
(f)
GLU26
ASN7
VAL2
(g)
(h)

Figure 5.

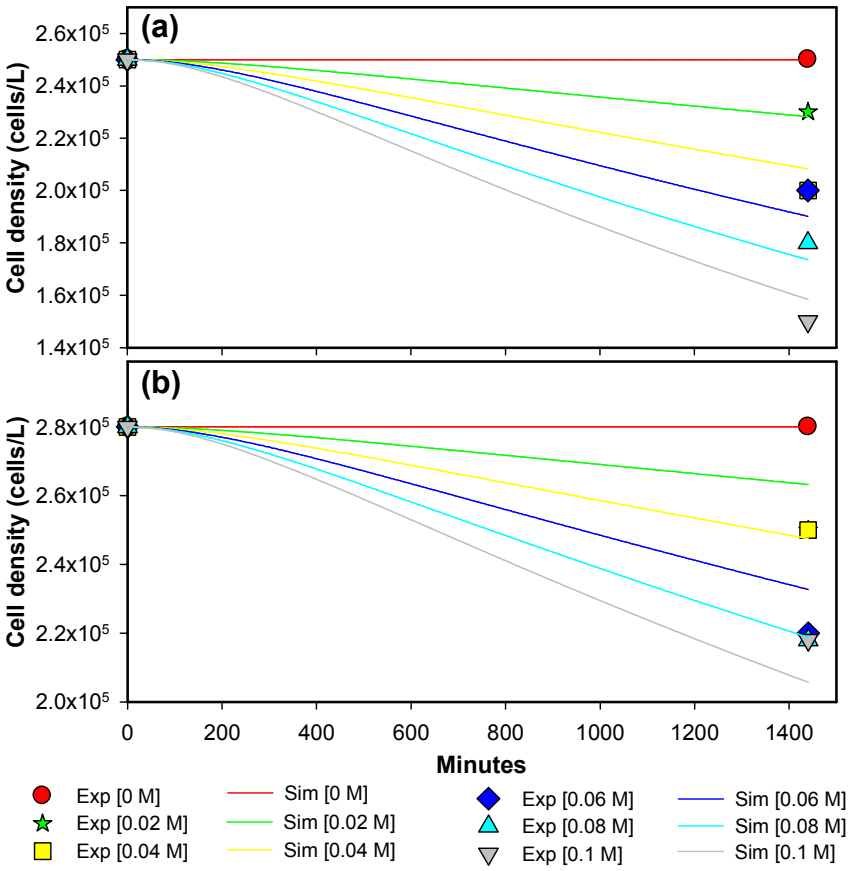
(a)
(b)
Cell density (cells/L)
2.6x10⁵
2.4x10⁵
2.2x10⁵
2.0x10⁵
1.8x10⁵
1.6x10⁵
1.4x10⁵
2.8x10⁵
2.6x10⁵
2.4x10⁵
2.2x10⁵
2.0x10⁵
0
200
400
600
800
1000
1200
1400
Minutes
Exp [0 M]
Exp [0.02 M]
Exp [0.04 M]
Sim [0 M]
Sim [0.02 M]
Sim [0.04 M]
Exp [0.06 M]
Exp [0.08 M]
Exp [0.1 M]
Sim [0.06 M]
Sim [0.08 M]
Sim [0.1 M]

Figure 6.

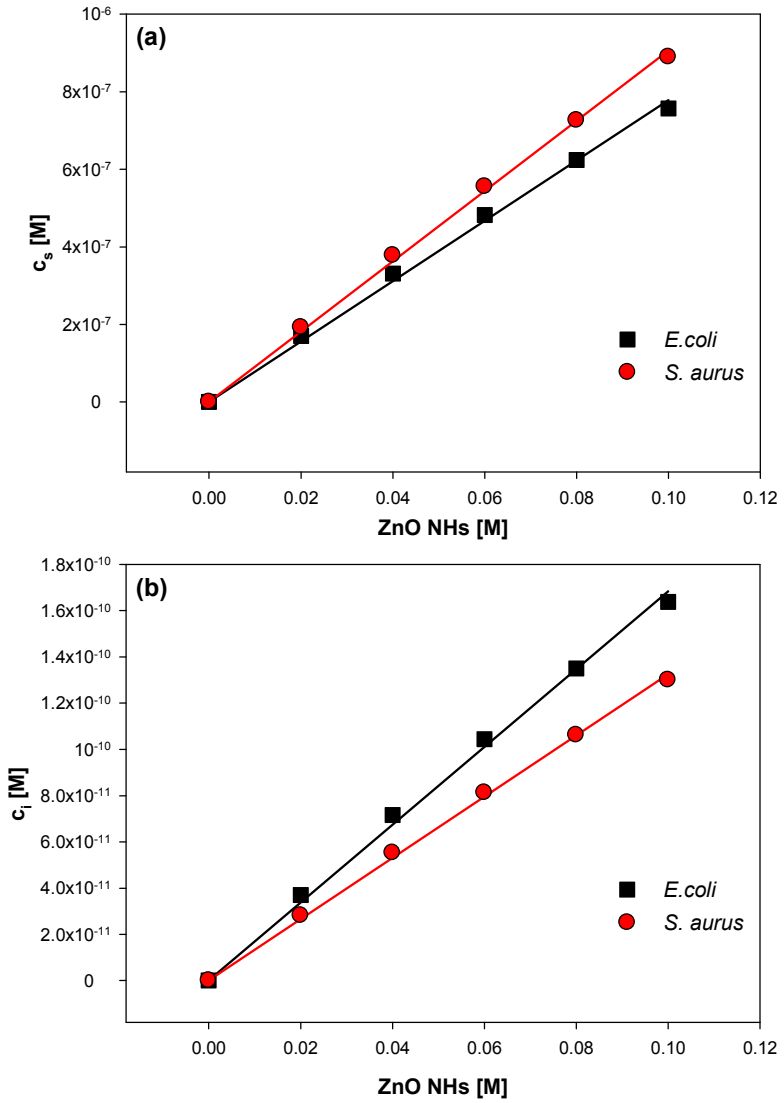
(a)
10^{-6}
$8x10^{-7}$
$6x10^{-7}$
$4x10^{-7}$
$2x10^{-7}$
0
c_s [M]
E.coli
S. aurus
0.00
0.02
0.04
0.06
0.08
0.10
0.12
ZnO NHs [M]
(b)
$1.8x10^{-10}$
$1.6x10^{-10}$
$1.4x10^{-10}$
$1.2x10^{-10}$
10^{-10}
$8.0x10^{-11}$
$6.0x10^{-11}$
$4.0x10^{-11}$
$2.0x10^{-11}$
0
c_i [M]
E.coli
S. aurus
0.00
0.02
0.04
0.06
0.08
0.10
0.12
ZnO NHs [M]

Graphical abstract